Appl. Math. Mech. -Engl. Ed., **42**(1), 65–84 (2021)

APPLIED MATHEMATICS AND MECHANICS (ENGLISH EDITION)

https://doi.org/10.1007/s10483-021-2672-8

Quantifying the parameter dependent basin of the unsafe regime of asymmetric Lévy-noise-induced critical transitions*

Jinzhong MA[1], Yong XU[2,3,†], Yongge LI[2], Ruilan TIAN[4], Shaojuan MA[5], J. KURTHS[6,7]

1. School of Mathematical Sciences, Shanxi University, Taiyuan 030000, China;
2. Department of Applied Mathematics, Northwestern Polytechnical University, Xi'an 710072, China;
3. MIIT Key Laboratory of Dynamics and Control of Complex Systems, Northwestern Polytechnical University, Xi'an 710072, China;
4. Department of Engineering Mechanics, Shijiazhuang Tiedao University, Shijiazhuang 050043, China;
5. School of Mathematics & Information Science, North Minzu University, Yinchuan 750021, China;
6. Potsdam Institute for Climate Impact Research, Potsdam 14412, Germany;
7. Department of Physics, Humboldt University at Berlin, Berlin 12489, Germany

(Received May 2, 2020 / Revised Jul. 15, 2020)

Abstract In real systems, the unpredictable jump changes of the random environment can induce the critical transitions (CTs) between two non-adjacent states, which are more catastrophic. Taking an asymmetric Lévy-noise-induced tri-stable model with desirable, sub-desirable, and undesirable states as a prototype class of real systems, a prediction of the noise-induced CTs from the desirable state directly to the undesirable one is carried out. We first calculate the region that the current state of the given model is absorbed into the undesirable state based on the escape probability, which is named as the absorbed region. Then, a new concept of the parameter dependent basin of the unsafe regime (PDBUR) under the asymmetric Lévy noise is introduced. It is an efficient tool for approximately quantifying the ranges of the parameters, where the noise-induced CTs from the desirable state directly to the undesirable one may occur. More importantly, it may provide theoretical guidance for us to adopt some measures to avert a noise-induced catastrophic CT.

* Citation: MA, J. Z., XU, Y., LI, Y. G., TIAN, R. L., MA, S. J., and KURTHS, J. Quantifying the parameter dependent basin of the unsafe regime of asymmetric Lévy-noise-induced critical transitions. *Applied Mathematics and Mechanics* (*English Edition*), **42**(1), 65–84 (2021) https://doi.org/10.1007/s10483-021-2672-8

† Corresponding author, E-mail: hsux3@nwpu.edu.cn

Project supported by the National Natural Science Foundation of China (No. 12072264), the Fundamental Research Funds for the Central Universities, the Research Funds for Interdisciplinary Subject of Northwestern Polytechnical University, the Shaanxi Project for Distinguished Young Scholars, the National Key Research and Development Program of China (No. 2018AAA0102201), and the Shaanxi Provincial Key R&D Program (Nos. 2020KW-013 and 2019TD-010)

Key words tri-stable model, asymmetric Lévy noise, critical transition (CT), escape probability, absorbed region, parameter dependent basin of unsafe regime (PDBUR)

Chinese Library Classification O175.13, O211.63, O29
2010 Mathematics Subject Classification 37H10, 37H20, 93E15

1 Introduction

Critical transition (CT) also called tipping, a phenomenon that a system shifts from one state to another contrasting one, is ubiquitous in many health and climate systems[1–4]. This sudden and often irreversible change may cause significant impacts on the local economy or society. Therefore, predicting CTs can be crucial for preventing such drastic changes. Using mathematical models of CTs, researchers have proposed various early warning signals to imminent CTs, such as variance and autocorrelation, phase lag, and amplitude difference[5–8]. However, their generality and applicability to practical systems have limitations because these models only contain one CT between two adjacent states.

In fact, many real systems may undergo multi-stable states with respect to gradually changing conditions. Typical examples include the endogenous molecular-cellular network[9], Earth's mass extinction[10], monsoon climate[11], and hypersonic boundary layer[12–13]. In these systems, CTs between non-adjacent states can occur due to large jumps in noisy environment, which may cause more catastrophic effects. For example, human cells may undergo healthy, sub-healthy, and cancer states[14]. When the cells of an organic tissue shift from a healthy state to a sub-healthy one, they still have a rather long time for the whole organism being viable. Now, the intervention of the treatment may recover the tissue to the healthy state. However, a physically strong body sometimes gets cancer suddenly, and the best time for a treatment is missed. This is actually a CT of cells from a healthy state directly to a cancer one. Hence, it is vitally important to warn jump changes induced CTs between non-adjacent states.

Random fluctuations-induced CTs have been often considered under the usual assumption of the Gaussian case, which describes small fluctuations in practice[15–17]. However, large jumps are always associated with a complex structure of the environment, which could not be described as the Gaussian noise. Therefore, a kind of the non-Gaussian noise needs to be considered to model unpredictable jumps of random environment. Lévy flights, a stochastic process characterized by the occurrence of extremely long jumps, can solve this problem[18–21]. The length of these jumps is distributed as Lévy stable statistics, which exhibits heavy tails and makes the moments divergent. So far, this kind of noise has been frequently encountered in nature, such as asset prices[22–23], protein folding[24], random search[25–26], Lagrangian drifts in certain oceanic fluid flows[27], and climate[28]. Compared with the Gaussian noise, the Lévy noise can induce a more catastrophic CT even between non-adjacent states. How to predict this type of CT, and then take measures to avert it is a problem we need to explore.

In Ref. [3], we have introduced the concept of parameter dependent basin of the unsafe regime (PDBUR) via the relationship between a Gaussian white noise-induced CT and the corresponding particle escaping. Using the same idea, in this paper, the PDBUR corresponding to Lévy-noise-induced CTs will be established. Then, the ranges of the parameters where Lévy-noise-induced CTs from the desirable state directly to the undesirable state may occur are quantified via this new concept.

Taking an asymmetric Lévy-noise-induced tri-stable model with desirable, sub-desirable, and undesirable states as a case study, the CT that may directly shift to the undesirable state and the corresponding escape problem of particles are first analyzed. Secondly, the different forms of the escape probability corresponding to different dynamic transitions are obtained. Then, the set that the current state of the given model is absorbed into the undesirable state is calculated, which is named as the absorbed region. Furthermore, the new concept of the PDBUR under asymmetric Lévy noise is introduced. Finally, some conclusions are presented to close this paper.

2 Model description

CTs between two non-adjacent states are widespread in various real-world systems. For example, a body may shift from a healthy state to a cancer state directly. Then, it is difficult to return to the healthy state even the sub-healthy state because the best time for a treatment is missing. To warn these catastrophic CTs between non-adjacent states, a self-constructed Lévy-noise-induced tri-stable model with desirable, sub-desirable, and undesirable states is considered. The form is

$$\frac{\mathrm{d}x}{\mathrm{d}t} = f(x,\varepsilon) + \frac{\mathrm{d}L_t}{\mathrm{d}t}, \tag{1}$$

where $f(x,\varepsilon) = -1.14x^5 - 0.4x^4 + 4.6x^3 + 0.5x^2 - 3.8x - \varepsilon$, ε is a control parameter, and these special coefficient values for $f(x,\varepsilon)$ are chosen to construct a basic model that roughly fits real systems[29]. L_t is a Lévy process with the generating triplet $(0, d, \sigma v_{\alpha,\beta})$, its time derivative is the Lévy noise, $v_{\alpha,\beta}$ is an asymmetric Lévy jump measure, and

$$v_{\alpha,\beta}(\mathrm{d}y) = \frac{C_1 I_{\{0<y<\infty\}}(y) + C_2 I_{\{-\infty<y<0\}}(y)}{|y|^{1+\alpha}}(\mathrm{d}y)$$

with

$$C_1 = C_\alpha \frac{1+\beta}{2}, \quad C_2 = C_\alpha \frac{1-\beta}{2}, \quad C_\alpha = \frac{\alpha(1-\alpha)}{\Gamma(2-\alpha)\cos\left(\frac{\pi\alpha}{2}\right)},$$

where $\Gamma(2-\alpha) = \int_0^{+\infty} t^{(2-\alpha)-1}\mathrm{e}^{-t}\mathrm{d}t$, $I_{\{.\}}$ denotes the indicator function, α is the stability index, and β is the skewness parameter[30]. We consider $\alpha \in (1,2)$ and $\beta \in [-1,0]$ throughout the paper.

In the absence of L_t, the system (1) can be reduced to the corresponding deterministic system, and the geometric structure of it versus ε is shown in Fig. 1. We find that there are five different regimes which have the following characteristics. The stable branches where x_{S1}, x_{S2}, and x_{S3} are located represent the desirable state, the sub-desirable state, and the undesirable state, respectively. Moreover, the unstable branches where x_{U1} and x_{U2} are located mark the height of the potential barrier between two adjacent stable branches. The coordinate values of Fold 1, Fold 2, Fold 3, and Fold 4 are $\varepsilon_{\text{Fold 1}} = 0.65$, $x_{\text{E-Fold 1}} = 1.343$, $\varepsilon_{\text{Fold 2}} = -1.26$, $x_{\text{E-Fold 2}} = 0.537$, $\varepsilon_{\text{Fold 3}} = 1.50$, $x_{\text{E-Fold 3}} = -0.586$, and $\varepsilon_{\text{Fold 4}} = -2.15$, $x_{\text{E-Fold 4}} = -1.576$, respectively.

Consider the large jumps in the Lévy noise, and three possible cases that the system (1) shifts directly to the undesirable state are also given in Fig. 1. They are CTs from the desirable

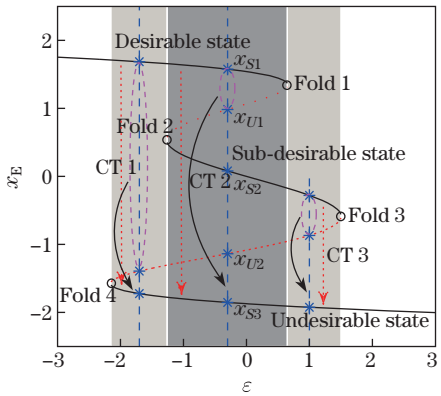

Fig. 1 The geometric structure of the deterministic system with respect to changing ε, where CT 1, CT 2, and CT 3 are three possible cases that the system (1) shifts directly to the undesirable state under the Lévy noise (color online)

state to the undesirable state in $\varepsilon \in [\varepsilon_{\text{Fold}\,4}, \varepsilon_{\text{Fold}\,2})$ and $\varepsilon \in [\varepsilon_{\text{Fold}\,2}, \varepsilon_{\text{Fold}\,1}]$, and CT from the sub-desirable state to the undesirable state in $\varepsilon \in (\varepsilon_{\text{Fold}\,1}, \varepsilon_{\text{Fold}\,3}]$. We record these three cases as CT 1, CT 2, and CT 3, respectively. Although both CT 1 and CT 2 shift from the desirable state to the undesirable state, the two states are adjacent for CT 1 and non-adjacent for CT 2. Similar to CT 1, the sub-desirable state and the undesirable state are also adjacent for CT 3.

From the perspective of noise-induced dynamic transitions, CT 1, CT 2, and CT 3 can correspond to three escape problems of particles, as follows:

Case 1 $\varepsilon \in [\varepsilon_{\text{Fold}\,4}, \varepsilon_{\text{Fold}\,2})$

Case 2 $\varepsilon \in [\varepsilon_{\text{Fold}\,2}, \varepsilon_{\text{Fold}\,1}]$

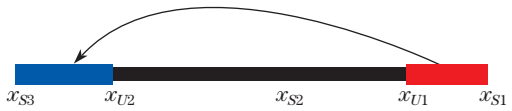

Case 3 $\varepsilon \in (\varepsilon_{\text{Fold}\,1}, \varepsilon_{\text{Fold}\,3}]$

Case 1 and Case 3 corresponding to CT 1 and CT 3 have the similar escape problems between two adjacent intervals, while Case 2 corresponding to CT 2 is the escape problem of particles between two non-adjacent intervals. Although $x \in [x_{U1}, x_{S1}]$ has left the current interval, the escape fails for CT 2 if x eventually falls in $[x_{U2}, x_{U1}]$.

In fact, a CT occurs when the current stable state is absorbed into another state. For example, Lévy-noise-induced CT 1 occurs because almost all $x \in [x_{U2}, x_{S1}]$ are absorbed into the undesirable state $[x_{S3}, x_{U2}]$. For a fixed $\varepsilon \in [\varepsilon_{\text{Fold}\,4}, \varepsilon_{\text{Fold}\,2})$, the possibility that a Lévy-noise-induced CT occurs can be estimated via measuring the part of $[x_{U2}, x_{S1}]$ that escapes to $[x_{S3}, x_{U2}]$. Similarly, for a fixed $\varepsilon \in [\varepsilon_{\text{Fold}\,2}, \varepsilon_{\text{Fold}\,1}]$ or $\varepsilon \in (\varepsilon_{\text{Fold}\,1}, \varepsilon_{\text{Fold}\,3}]$, the part of $[x_{U1}, x_{S1}]$ or $[x_{U2}, x_{S2}]$ that is absorbed into $[x_{S3}, x_{U2}]$ should be quantified. Here, we quantify the absorbed region of the current interval via analyzing the escape probability, and the different forms of the escape probability corresponding to Cases 1, 2, and 3 will be obtained below.

3 Escape probability

For any $u(x) \in H_0^2(\mathbf{R})$, the generator of the stochastic process x of the system (1) is

$$\begin{aligned} L_2 u(x) = & \frac{d}{2} u''(x) + f(x, \varepsilon)\, u'(x) \\ & + \sigma \int_{\mathbf{R}\setminus\{0\}} \left(u(x+y) - u(x) - I_{\{|y|<1\}}(y)\, y u'(x) \right) v_{\alpha,\beta}(\mathrm{d}y), \end{aligned} \tag{2}$$

where d is the intensity of Gaussian noise, and σ is the intensity of Lévy noise. $u'(x)$ and $u''(x)$ represent the first and second derivatives of $u(x)$ versus x, respectively. Note that y belongs to the symmetry interval $(-1, 1)$ in the de-singularizing term $I_{|y|<1}(y) y u'(x)$. However, the range of y is generally an asymmetric interval (a, b).

Suppose that x belongs to a general interval (a,b). Then, δ in $I_{|y|<1}(y)yu'(x)$ is no longer equal to 1. From the following derivation process, we find $\delta=(b-a)/2$. Hence, we first replace $I_{\{|y|<1\}}(y)$ in Eq. (2) to $I_{\{|y|<(b-a)/2\}}(y)$ and get

$$\frac{d}{2}u''(x)+c(x)u'(x)+\sigma\int_{\mathbf{R}\setminus\{0\}}\big(u(x+y)-u(x)-I_{\{|y|<\frac{b-a}{2}\}}(y)yu'(x)\big)v_{\alpha,\beta}(\mathrm{d}y)=0, \quad (3)$$

where

$$c(x)=f(x,\varepsilon)+\sigma(C_1-C_2)\frac{\left(\frac{b-a}{2}\right)^{1-\alpha}-1}{1-\alpha}.$$

Next, the different forms of the escape probability corresponding to Cases 1, 2, and 3 will be derived based on Eq. (3).

3.1 Case 1 or Case 3

The asymmetric Lévy-noise-induced CT 1 and CT 3 have the same form of the escape problem as follows:

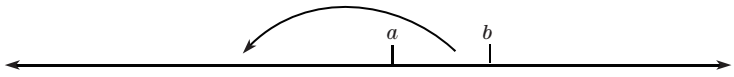

Here, $(a,b)=(x_{U2},x_{S1})$ for CT 1 and $(a,b)=(x_{U2},x_{S2})$ for CT 3. If $u(x)$ is regarded as the escape probability, then $u(x)=0$ for $x\in[b,\infty)$ and $u(x)=1$ for $x\in(-\infty,a]$. To keep the computational domain fixed as $(-1,1)$, we perform a scalar conversion,

$$x=\frac{b-a}{2}z+\frac{b+a}{2},$$

where $z\in(-1,1)$.

Defining

$$v(z)=u\Big(\frac{b-a}{2}z+\frac{b+a}{2}\Big),$$

we get

$$\frac{\mathrm{d}u}{\mathrm{d}x}=\frac{2}{b-a}\frac{\mathrm{d}v}{\mathrm{d}z},\quad \frac{\mathrm{d}^2u}{\mathrm{d}x^2}=\frac{4}{(b-a)^2}\frac{\mathrm{d}^2v}{\mathrm{d}z^2}.$$

Let $\widehat{y}=\frac{2}{b-a}y$. Then, the integral term in Eq. (3) can be rewritten as

$$\Big(\frac{2}{b-a}\Big)^{\alpha}\int_{\mathbf{R}\setminus\{0\}}\big(v(z+\widehat{y})-v(z)-I_{\{|\widehat{y}|<1\}}\widehat{y}v'(z)\big)\frac{C_1I_{\{0<\widehat{y}<\infty\}}(\widehat{y})+C_2I_{\{-\infty<\widehat{y}<0\}}(\widehat{y})}{|\widehat{y}|^{1+\alpha}}(\mathrm{d}\widehat{y}),$$

where $v'(z)$ is the first derivative of $v(z)$ versus z.

Therefore, the equivalent form of Eq. (3) is

$$\sigma\Big(\frac{2}{b-a}\Big)^{\alpha}\int_{\mathbf{R}\setminus\{0\}}\big(v(z+\widehat{y})-v(z)-I_{\{|\widehat{y}|<1\}}\widehat{y}v'(z)\big)\frac{C_1I_{\{0<\widehat{y}<\infty\}}(\widehat{y})+C_2I_{\{-\infty<\widehat{y}<0\}}(\widehat{y})}{|\widehat{y}|^{1+\alpha}}(\mathrm{d}\widehat{y})$$
$$+\frac{4}{(b-a)^2}\frac{d}{2}v''(z)+\frac{2}{b-a}c\Big(\frac{b-a}{2}z+\frac{b+a}{2}\Big)v'(z)=0, \quad (4)$$

where $v''(z)$ is the second derivative of $v(z)$ versus z.

Due to $v(z)=0$ for $z\in[1,\infty)$ and $v(z)=1$ for $z\in(-\infty,-1]$, we can further infer that $v(z+\widehat{y})=0$ when $\widehat{y}\geqslant 1-z$, and $v(z+\widehat{y})=1$ when $\widehat{y}\leqslant -1-z$.

Suppose that the integral in Eq. (4) is denoted by I_0,

$$I_0=\int_{\mathbf{R}\setminus\{0\}}\left(v\left(z+\widehat{y}\right)-v\left(z\right)-I_{\{|\widehat{y}|<1\}}\widehat{y}v'\left(z\right)\right)\frac{C_1I_{\{0<\widehat{y}<\infty\}}\left(\widehat{y}\right)+C_2I_{\{-\infty<\widehat{y}<0\}}\left(\widehat{y}\right)}{\left|\widehat{y}\right|^{1+\alpha}}\left(\mathrm{d}\widehat{y}\right).$$

We decompose $I_0=C_1I_1+C_2I_2$, where

$$I_1=\int_{\mathbf{R}^+}\frac{v\left(z+\widehat{y}\right)-v\left(z\right)-I_{\{|\widehat{y}|<1\}}\widehat{y}v'\left(z\right)}{\widehat{y}^{1+\alpha}}\left(\mathrm{d}\widehat{y}\right),$$
$$I_2=\int_{\mathbf{R}^-}\frac{v\left(z+\widehat{y}\right)-v\left(z\right)-I_{\{|\widehat{y}|<1\}}\widehat{y}v'\left(z\right)}{\left|\widehat{y}\right|^{1+\alpha}}\left(\mathrm{d}\widehat{y}\right).$$

I_1 can be rewritten as

$$I_1=\int_0^1\frac{v\left(z+\widehat{y}\right)-v\left(z\right)-\widehat{y}v'\left(z\right)}{\widehat{y}^{1+\alpha}}\left(\mathrm{d}\widehat{y}\right)+\int_1^\infty\frac{v\left(z+\widehat{y}\right)-v\left(z\right)}{\widehat{y}^{1+\alpha}}\left(\mathrm{d}\widehat{y}\right).$$

For $z>0$, we have

$$\begin{aligned}I_1&=\int_0^{1-z}\frac{v\left(z+\widehat{y}\right)-v\left(z\right)-\widehat{y}v'\left(z\right)}{\widehat{y}^{1+\alpha}}\left(\mathrm{d}\widehat{y}\right)+\frac{v\left(z\right)}{\alpha}(1-(1-z)^{-\alpha})-v'\left(z\right)\frac{1-(1-z)^{1-\alpha}}{1-\alpha}-\frac{v\left(z\right)}{\alpha}\\&=-\frac{v\left(z\right)}{\alpha}\left(1-z\right)^{-\alpha}-v'\left(z\right)\frac{1-(1-z)^{1-\alpha}}{1-\alpha}+\int_0^{1-z}\frac{v\left(z+\widehat{y}\right)-v\left(z\right)-\widehat{y}v'\left(z\right)}{\widehat{y}^{1+\alpha}}\left(\mathrm{d}\widehat{y}\right).\end{aligned}$$

For $z<0$, we get

$$I_1=-\frac{v\left(z\right)}{\alpha}\left(1-z\right)^{-\alpha}+\int_1^{1-z}\frac{v\left(z+\widehat{y}\right)-v\left(z\right)}{\widehat{y}^{1+\alpha}}\left(\mathrm{d}\widehat{y}\right)+\int_0^1\frac{v\left(z+\widehat{y}\right)-v\left(z\right)-\widehat{y}v'\left(z\right)}{\widehat{y}^{1+\alpha}}\left(\mathrm{d}\widehat{y}\right).$$

I_2 can be rewritten as

$$I_2=\int_{-1}^0\frac{v\left(z+\widehat{y}\right)-v\left(z\right)-\widehat{y}v'\left(z\right)}{\left|\widehat{y}\right|^{1+\alpha}}\left(\mathrm{d}\widehat{y}\right)+\int_{-\infty}^{-1}\frac{v\left(z+\widehat{y}\right)-v\left(z\right)}{\left|\widehat{y}\right|^{1+\alpha}}\left(\mathrm{d}\widehat{y}\right).$$

For $z>0$, we have

$$I_2=\frac{1-v\left(z\right)}{\alpha}\left(1+z\right)^{-\alpha}+\int_{-1-z}^{-1}\frac{v\left(z+\widehat{y}\right)-v\left(z\right)}{\left(-\widehat{y}\right)^{1+\alpha}}\left(\mathrm{d}\widehat{y}\right)+\int_{-1}^0\frac{v\left(z+\widehat{y}\right)-v\left(z\right)-\widehat{y}v'\left(z\right)}{\left(-\widehat{y}\right)^{1+\alpha}}\left(\mathrm{d}\widehat{y}\right).$$

For $z<0$, we get

$$\begin{aligned}I_2&=\frac{v\left(z\right)-1}{\alpha}(1-(1+z)^{-\alpha})+v'\left(z\right)\frac{1-(1+z)^{1-\alpha}}{1-\alpha}\\&\quad+\int_{-1-z}^0\frac{v\left(z+\widehat{y}\right)-v\left(z\right)-\widehat{y}v'\left(z\right)}{\left(-\widehat{y}\right)^{1+\alpha}}\left(\mathrm{d}\widehat{y}\right)+\frac{1-v\left(z\right)}{\alpha}\\&=\frac{1-v\left(z\right)}{\alpha}\left(1+z\right)^{-\alpha}+v'\left(z\right)\frac{1-(1+z)^{1-\alpha}}{1-\alpha}+\int_{-1-z}^0\frac{v\left(z+\widehat{y}\right)-v\left(z\right)-\widehat{y}v'\left(z\right)}{\left(-\widehat{y}\right)^{1+\alpha}}\left(\mathrm{d}\widehat{y}\right).\end{aligned}$$

Combining the above results of I_1 and I_2, we rewrite Eq. (4) as

$$\begin{aligned}
&\sigma\Big(\frac{2}{b-a}\Big)^{\alpha}\bigg(C_1\int_0^{1-z}\frac{v\left(z+\widehat{y}\right)-v\left(z\right)-\widehat{y}v'\left(z\right)}{\widehat{y}^{1+\alpha}}\left(\mathrm{d}\widehat{y}\right)+C_2\bigg(\int_{-1-z}^{-1}\frac{v\left(z+\widehat{y}\right)-v\left(z\right)}{\left(-\widehat{y}\right)^{1+\alpha}}\left(\mathrm{d}\widehat{y}\right)\\
&+\int_{-1}^{0}\frac{v\left(z+\widehat{y}\right)-v\left(z\right)-\widehat{y}v'\left(z\right)}{\left(-\widehat{y}\right)^{1+\alpha}}\left(\mathrm{d}\widehat{y}\right)\bigg)\bigg)+\bigg(\frac{2}{b-a}\bigg(f\Big(\frac{b-a}{2}z+\frac{b+a}{2},\varepsilon\Big)\\
&+\sigma\left(C_1-C_2\right)\frac{\left(\frac{b-a}{2}\right)^{1-\alpha}-1}{1-\alpha}\bigg)-\sigma\Big(\frac{2}{b-a}\Big)^{\alpha}C_1\frac{1-\left(1-z\right)^{1-\alpha}}{1-\alpha}\bigg)v'\left(z\right)\\
&-\sigma\Big(\frac{2}{b-a}\Big)^{\alpha}\frac{v\left(z\right)}{\alpha}\big(C_1\left(1-z\right)^{-\alpha}+C_2\left(1+z\right)^{-\alpha}\big)+\frac{4}{\left(b-a\right)^2}\frac{d}{2}v''\left(z\right)\\
=&-\frac{\sigma C_2}{\alpha}\Big(\frac{2}{b-a}\Big)^{\alpha}\frac{1}{\left(1+z\right)^{\alpha}}\quad\text{for}\quad z\geqslant 0,
\end{aligned}\tag{5}$$

while

$$\begin{aligned}
&\sigma\Big(\frac{2}{b-a}\Big)^{\alpha}\bigg(C_1\bigg(\int_0^{1}\frac{v\left(z+\widehat{y}\right)-v\left(z\right)-\widehat{y}v'\left(z\right)}{\widehat{y}^{1+\alpha}}\left(\mathrm{d}\widehat{y}\right)+\int_1^{1-z}\frac{v\left(z+\widehat{y}\right)-v\left(z\right)}{\widehat{y}^{1+\alpha}}\left(\mathrm{d}\widehat{y}\right)\bigg)\\
&+C_2\int_{-1-z}^{0}\frac{v\left(z+\widehat{y}\right)-v\left(z\right)-\widehat{y}v'\left(z\right)}{\left(-\widehat{y}\right)^{1+\alpha}}\left(\mathrm{d}\widehat{y}\right)\bigg)+\Big(\frac{2}{b-a}\Big(f\Big(\frac{b-a}{2}z+\frac{b+a}{2},\varepsilon\Big)\\
&+\sigma\left(C_1-C_2\right)\frac{\left(\frac{b-a}{2}\right)^{1-\alpha}-1}{1-\alpha}\Big)+\sigma\Big(\frac{2}{b-a}\Big)^{\alpha}C_2\frac{1-\left(1+z\right)^{1-\alpha}}{1-\alpha}\Big)v'\left(z\right)\\
&-\sigma\Big(\frac{2}{b-a}\Big)^{\alpha}\frac{v\left(z\right)}{\alpha}\big(C_1\left(1-z\right)^{-\alpha}+C_2\left(1+z\right)^{-\alpha}\big)+\frac{4}{\left(b-a\right)^2}\frac{d}{2}v''\left(z\right)\\
=&-\frac{\sigma C_2}{\alpha}\Big(\frac{2}{b-a}\Big)^{\alpha}\frac{1}{\left(1+z\right)^{\alpha}}\quad\text{for}\quad z<0.
\end{aligned}\tag{6}$$

Next, Eqs. (5) and (6) are discretized. We divide the computational domain $[-1,1]$ into $2J$ subintervals, i.e., $z_j=jh$, $-J\leqslant j\leqslant J$ with each subinterval having the size $h=1/J$. Denote the numerical solution by the vector $V=V_{-J:J}$, where the component V_j approximates $v_j\equiv v(z_j)$ for $-J\leqslant j\leqslant J$. Then, the discretizations corresponding to Eqs. (5) and (6) are

$$\begin{aligned}
&\sigma\Big(\frac{2}{b-a}\Big)^{\alpha}\bigg(C_1h{\sum_{k=1}^{J-j}}'\frac{V_{j+k}-V_j-z_k\frac{V_{j+1}-V_{j-1}}{2h}}{\left|z_k\right|^{1+\alpha}}+C_2h\bigg({\sum_{k=-J}^{-1}}''\frac{V_{j+k}-V_j-z_k\frac{V_{j+1}-V_{j-1}}{2h}}{\left|z_k\right|^{1+\alpha}}\\
&+\sum_{k=-J-j}^{-J}\frac{V_{j+k}-V_j}{\left|z_k\right|^{1+\alpha}}\bigg)\bigg)+\Big(\frac{2}{b-a}\Big(f\Big(\frac{b-a}{2}z_j+\frac{b+a}{2},\varepsilon\Big)+\sigma(C_1-C_2)\frac{\left(\frac{b-a}{2}\right)^{1-\alpha}-1}{1-\alpha}\Big)\\
&-\sigma\Big(\frac{2}{b-a}\Big)^{\alpha}C_1\frac{1-\left(1-z_j\right)^{1-\alpha}}{1-\alpha}\Big)\frac{V_{j+1}-V_{j-1}}{2h}-\sigma\Big(\frac{2}{b-a}\Big)^{\alpha}\frac{V_j}{\alpha}(C_1(1-z_j)^{-\alpha}+C_2\left(1+z_j\right)^{-\alpha})\\
&+\frac{4}{\left(b-a\right)^2}\frac{d}{2}\frac{V_{j+1}-2V_j+V_{j-1}}{h^2}=-\frac{\sigma C_2}{\alpha}\Big(\frac{2}{b-a}\Big)^{\alpha}\frac{1}{\left(1+z_j\right)^{\alpha}}\quad\text{for}\quad 0\leqslant j\leqslant J-1,
\end{aligned}\tag{7}$$

while

$$\begin{aligned}
&\sigma\Big(\frac{2}{b-a}\Big)^{\alpha}\Big(C_1h\Big(\sum_{k=1}^{J}{}'\frac{V_{j+k}-V_j-z_k\frac{V_{j+1}-V_{j-1}}{2h}}{|z_k|^{1+\alpha}}+\sum_{k=J}^{J-j}\frac{V_{j+k}-V_j}{|z_k|^{1+\alpha}}\Big)\\
&+C_2h\sum_{k=-J-j}^{-1}{}''\frac{V_{j+k}-V_j-z_k\frac{V_{j+1}-V_{j-1}}{2h}}{|z_k|^{1+\alpha}}\Big)+\Big(\frac{2}{b-a}\Big(f\Big(\frac{b-a}{2}z_j+\frac{b+a}{2},\varepsilon\Big)\\
&+\sigma\left(C_1-C_2\right)\frac{\left(\frac{b-a}{2}\right)^{1-\alpha}-1}{1-\alpha}\Big)+\sigma\Big(\frac{2}{b-a}\Big)^{\alpha}C_2\frac{1-(1+z_j)^{1-\alpha}}{1-\alpha}\Big)\frac{V_{j+1}-V_{j-1}}{2h}\\
&-\sigma\Big(\frac{2}{b-a}\Big)^{\alpha}\frac{V_j}{\alpha}(C_1(1-z_j)^{-\alpha}+C_2(1+z_j)^{-\alpha})+\frac{4}{(b-a)^2}\frac{d}{2}\frac{V_{j+1}-2V_j+V_{j-1}}{h^2}\\
&=-\frac{\sigma C_2}{\alpha}\Big(\frac{2}{b-a}\Big)^{\alpha}\frac{1}{(1+z_j)^{\alpha}}\quad\text{for}\quad -J+1\leqslant j\leqslant -1,
\end{aligned}\tag{8}$$

where the summation symbol $\sum$ means that the terms of both end indices are multiplied by $1/2$, $\sum''$ means that only the term of the bottom index is multiplied by $1/2$, and $\sum'$ means that only the term of the upper index is multiplied by $1/2$.

The truncation errors of the central difference schemes for the derivatives in Eqs. (7) and (8) are of the second-order $O(h^2)$. From the error analysis of Refs. [31] and [32], the leading-order error of the quadrature rule is

$$-\sigma\Big(\frac{2}{b-a}\Big)^{\alpha}\left(C_1+C_2\right)\zeta\left(\alpha-1\right)\frac{v''\left(z\right)}{2}h^{2-\alpha}=-\sigma\Big(\frac{2}{b-a}\Big)^{\alpha}C_{\alpha}\zeta\left(\alpha-1\right)\frac{v''\left(z\right)}{2}h^{2-\alpha},$$

where ζ is the Riemann zeta function. Then, Eqs. (7) and (8) can be further written as

$$\begin{aligned}
&\sigma\left(\frac{2}{b-a}\right)^{\alpha}\Big(C_1h\sum_{k=1}^{J-j}{}'\frac{V_{j+k}-V_j-z_k\frac{V_{j+1}-V_{j-1}}{2h}}{|z_k|^{1+\alpha}}\\
&+C_2h\Big(\sum_{k=-J}^{-1}{}''\frac{V_{j+k}-V_j-z_k\frac{V_{j+1}-V_{j-1}}{2h}}{|z_k|^{1+\alpha}}+\sum_{k=-J-j}^{-J}\frac{V_{j+k}-V_j}{|z_k|^{1+\alpha}}\Big)\Big)\\
&+\Big(\frac{2}{b-a}\Big(f\Big(\frac{b-a}{2}z_j+\frac{b+a}{2},\varepsilon\Big)+\sigma\left(C_1-C_2\right)\frac{\left(\frac{b-a}{2}\right)^{1-\alpha}-1}{1-\alpha}\Big)\\
&-\sigma\Big(\frac{2}{b-a}\Big)^{\alpha}C_1\frac{1-(1-z_j)^{1-\alpha}}{1-\alpha}\Big)\frac{V_{j+1}-V_{j-1}}{2h}+\Big(\frac{4}{(b-a)^2}\frac{d}{2}-\sigma\Big(\frac{2}{b-a}\Big)^{\alpha}\\
&\cdot C_{\alpha}\zeta(\alpha-1)\frac{1}{2}h^{2-\alpha}\Big)\frac{V_{j+1}-2V_j+V_{j-1}}{h^2}-\sigma\Big(\frac{2}{b-a}\Big)^{\alpha}\frac{V_j}{\alpha}(C_1(1-z_j)^{-\alpha}\\
&+C_2(1+z_j)^{-\alpha})=-\frac{\sigma C_2}{\alpha}\Big(\frac{2}{b-a}\Big)^{\alpha}\frac{1}{(1+z_j)^{\alpha}}\quad\text{for}\quad 0\leqslant j\leqslant J-1,
\end{aligned}\tag{9}$$

while

$$\begin{aligned}
&\sigma\Big(\frac{2}{b-a}\Big)^{\alpha}\Big(C_1h\Big(\sum_{k=1}^{J}{}'\frac{V_{j+k}-V_j-z_k\frac{V_{j+1}-V_{j-1}}{2h}}{|z_k|^{1+\alpha}}+\sum_{k=J}^{J-j}\frac{V_{j+k}-V_j}{|z_k|^{1+\alpha}}\Big)\\
&+C_2h\sum_{k=-J-j}^{-1}{}''\frac{V_{j+k}-V_j-z_k\frac{V_{j+1}-V_{j-1}}{2h}}{|z_k|^{1+\alpha}}\Big)+\Big(\frac{2}{b-a}\Big(f\Big(\frac{b-a}{2}z_j+\frac{b+a}{2},\varepsilon\Big)
\end{aligned}$$

$$+\sigma(C_1-C_2)\frac{\left(\frac{b-a}{2}\right)^{1-\alpha}-1}{1-\alpha}\Big)+\sigma\Big(\frac{2}{b-a}\Big)^{\alpha}C_2\frac{1-(1+z_j)^{1-\alpha}}{1-\alpha}\Big)\frac{V_{j+1}-V_{j-1}}{2h}$$
$$+\Big(\frac{4}{(b-a)^2}\frac{d}{2}-\sigma\Big(\frac{2}{b-a}\Big)^{\alpha}C_\alpha\zeta(\alpha-1)\frac{1}{2}h^{2-\alpha}\Big)\frac{V_{j+1}-2V_j+V_{j-1}}{h^2}-\sigma\Big(\frac{2}{b-a}\Big)^{\alpha}$$
$$\cdot\frac{V_j}{\alpha}(C_1(1-z_j)^{-\alpha}+C_2(1+z_j)^{-\alpha})=-\frac{\sigma C_2}{\alpha}\Big(\frac{2}{b-a}\Big)^{\alpha}\frac{1}{(1+z_j)^{\alpha}}\quad\text{for}\quad -J+1\leqslant j\leqslant -1. \quad (10)$$

By taking (a,b) as (x_{U2},x_{S1}) under a fixed $\varepsilon\in[\varepsilon_{\text{Fold}\,4},\varepsilon_{\text{Fold}\,2})$, $V_{-J}=1$ and $V_J=0$, the escape probability $V\triangleq P_1(x)$ corresponding to CT 1 can be obtained via Eqs. (9) and (10). Similarly, the escape probability $V\triangleq P_3(x)$ corresponding to CT 3 can be obtained when (a,b) is taken as (x_{U2},x_{S2}) under a fixed $\varepsilon\in[\varepsilon_{\text{Fold}\,1},\varepsilon_{\text{Fold}\,3})$.

3.2 Case 2

For the asymmetric Lévy-noise-induced CT 2, there is an interval $[x_{U2},x_{U1}]$ between the two non-adjacent intervals (x_{U1},x_{S1}) and $[x_{S3},x_{U2}]$. Let (x_{U1},x_{S1}) be (a,b) and $[x_{S3},x_{U2}]$ be $(\widehat{c},\widehat{d})$. Then, $\widehat{c}<\widehat{d}<a<b$, and the corresponding dynamic transition is as follows:

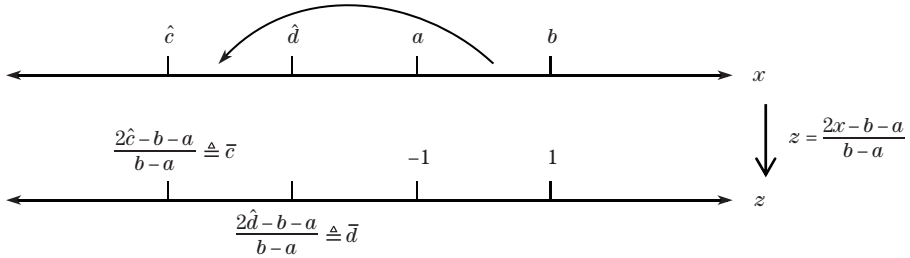

We have transformed $x\in(a,b)$ to $z\in(-1,1)$ via $x=\frac{b-a}{2}z+\frac{b+a}{2}$ above[33]. Based on this scalar conversion, the value corresponding to $(\widehat{c},\widehat{d})$ on the z-axis can be obtained, leading to $\big(\frac{2\widehat{c}-b-a}{b-a},\frac{2\widehat{d}-b-a}{b-a}\big)\triangleq(\overline{c},\overline{d})$. Because $v(z)=0$ for $z\in[1,\infty)\cup(\overline{d},-1)$ and $v(z)=1$ for $z\in(-\infty,\overline{d}]$, we can further infer that $v(z+\widehat{y})=0$ when $\widehat{y}\geqslant 1-z$ or $\overline{d}-z<\widehat{y}<-1-z$ and $v(z+\widehat{y})=1$ when $\widehat{y}\leqslant\overline{d}-z$.

Similar to CT 1 and CT 3, the integral in Eq. (4) is denoted by I_0,

$$I_0=\int_{\mathbf{R}\setminus\{0\}}\left(v\left(z+\widehat{y}\right)-v\left(z\right)-I_{\{|\widehat{y}|<1\}}\widehat{y}v'\left(z\right)\right)\frac{C_1I_{\{0<\widehat{y}<\infty\}}\left(\widehat{y}\right)+C_2I_{\{-\infty<\widehat{y}<0\}}\left(\widehat{y}\right)}{|\widehat{y}|^{1+\alpha}}\left(\mathrm{d}\widehat{y}\right).$$

We decompose $I_0=C_1I_1+C_2I_2$, where

$$I_1=\int_{\mathbf{R}^+}\frac{v\left(z+\widehat{y}\right)-v\left(z\right)-I_{\{|\widehat{y}|<1\}}\widehat{y}v'\left(z\right)}{\widehat{y}^{1+\alpha}}\left(\mathrm{d}\widehat{y}\right),$$
$$I_2=\int_{\mathbf{R}^-}\frac{v\left(z+\widehat{y}\right)-v\left(z\right)-I_{\{|\widehat{y}|<1\}}\widehat{y}v'\left(z\right)}{|\widehat{y}|^{1+\alpha}}\left(\mathrm{d}\widehat{y}\right).$$

Since I_1 here is the same as I_1 of Case 1 or Case 3, we only need to analyze I_2,

$$I_2=\int_{-1}^{0}\frac{v\left(z+\widehat{y}\right)-v\left(z\right)-\widehat{y}v'\left(z\right)}{|\widehat{y}|^{1+\alpha}}\left(\mathrm{d}\widehat{y}\right)+\int_{-\infty}^{-1}\frac{v\left(z+\widehat{y}\right)-v\left(z\right)}{|\widehat{y}|^{1+\alpha}}\left(\mathrm{d}\widehat{y}\right).$$

For $z>0$, we get

$$I_2=\frac{1}{\alpha}\left(z-\overline{d}\right)^{-\alpha}-\frac{v\left(z\right)}{\alpha}\left(1+z\right)^{-\alpha}+\int_{-1-z}^{-1}\frac{v\left(z+\widehat{y}\right)-v\left(z\right)}{\left(-\widehat{y}\right)^{1+\alpha}}\left(\mathrm{d}\widehat{y}\right)$$
$$+\int_{-1}^{0}\frac{v\left(z+\widehat{y}\right)-v\left(z\right)-\widehat{y}v'\left(z\right)}{\left(-\widehat{y}\right)^{1+\alpha}}\left(\mathrm{d}\widehat{y}\right).$$

For $z<0$, we have

$$\begin{aligned}I_2=&\frac{v(z)}{\alpha}(1-(1+z)^{-\alpha})+v'(z)\frac{1-(1+z)^{1-\alpha}}{1-\alpha}\\&+\int_{-1-z}^{0}\frac{v(z+\widehat{y})-v(z)-\widehat{y}v'(z)}{(-\widehat{y})^{1+\alpha}}(\mathrm{d}\widehat{y})+\frac{1}{\alpha}\left(z-\overline{d}\right)^{-\alpha}-\frac{v(z)}{\alpha}\\=&-\frac{v(z)}{\alpha}(1+z)^{-\alpha}+v'(z)\frac{1-(1+z)^{1-\alpha}}{1-\alpha}+\frac{1}{\alpha}\left(z-\overline{d}\right)^{-\alpha}\\&+\int_{-1-z}^{0}\frac{v(z+\widehat{y})-v(z)-\widehat{y}v'(z)}{(-\widehat{y})^{1+\alpha}}(\mathrm{d}\widehat{y}).\end{aligned}$$

Combining the above results of I_1 and I_2, we rewrite Eq. (4) as

$$\begin{aligned}&\sigma\Big(\frac{2}{b-a}\Big)^{\alpha}\left(C_1\int_{0}^{1-z}\frac{v(z+\widehat{y})-v(z)-\widehat{y}v'(z)}{\widehat{y}^{1+\alpha}}(\mathrm{d}\widehat{y})\right.\\&\left.+C_2\left(\int_{-1-z}^{-1}\frac{v(z+\widehat{y})-v(z)}{(-\widehat{y})^{1+\alpha}}(\mathrm{d}\widehat{y})+\int_{-1}^{0}\frac{v(z+\widehat{y})-v(z)-\widehat{y}v'(z)}{(-\widehat{y})^{1+\alpha}}(\mathrm{d}\widehat{y})\right)\right)\\&+\Big(\frac{2}{b-a}\Big(f\Big(\frac{b-a}{2}z+\frac{b+a}{2},\varepsilon\Big)+\sigma(C_1-C_2)\frac{\left(\frac{b-a}{2}\right)^{1-\alpha}-1}{1-\alpha}\Big)\\&-\sigma\Big(\frac{2}{b-a}\Big)^{\alpha}C_1\frac{1-(1-z)^{1-\alpha}}{1-\alpha}\Big)v'(z)\\&-\sigma\Big(\frac{2}{b-a}\Big)^{\alpha}\frac{v(z)}{\alpha}(C_1(1-z)^{-\alpha}+C_2(1+z)^{-\alpha})+\frac{4}{(b-a)^2}\frac{d}{2}v''(z)\\=&-\frac{\sigma C_2}{\alpha}\Big(\frac{2}{b-a}\Big)^{\alpha}(z-\overline{d})^{-\alpha}\quad\text{for}\quad z\geqslant 0,\end{aligned}\tag{11}$$

while

$$\begin{aligned}&\sigma\Big(\frac{2}{b-a}\Big)^{\alpha}\left(C_1\left(\int_{0}^{1}\frac{v(z+\widehat{y})-v(z)-\widehat{y}v'(z)}{\widehat{y}^{1+\alpha}}(\mathrm{d}\widehat{y})+\int_{1}^{1-z}\frac{v(z+\widehat{y})-v(z)}{\widehat{y}^{1+\alpha}}(\mathrm{d}\widehat{y})\right)\right.\\&\left.+C_2\int_{-1-z}^{0}\frac{v(z+\widehat{y})-v(z)-\widehat{y}v'(z)}{(-\widehat{y})^{1+\alpha}}(\mathrm{d}\widehat{y})\right)+\Big(\frac{2}{b-a}\Big(f\Big(\frac{b-a}{2}z+\frac{b+a}{2},\varepsilon\Big)\\&+\sigma(C_1-C_2)\frac{\left(\frac{b-a}{2}\right)^{1-\alpha}-1}{1-\alpha}\Big)+\sigma\Big(\frac{2}{b-a}\Big)^{\alpha}C_2\frac{1-(1+z)^{1-\alpha}}{1-\alpha}\Big)v'(z)\\&-\sigma\Big(\frac{2}{b-a}\Big)^{\alpha}\frac{v(z)}{\alpha}(C_1(1-z)^{-\alpha}+C_2(1+z)^{-\alpha})+\frac{4}{(b-a)^2}\frac{d}{2}v''(z)\\=&-\frac{\sigma C_2}{\alpha}\Big(\frac{2}{b-a}\Big)^{\alpha}(z-\overline{d})^{-\alpha}\quad\text{for}\quad z<0.\end{aligned}\tag{12}$$

Using the same discretization method in Case 1 or Case 3, the discretizations corresponding to Eqs. (11) and (12) are

$$\begin{aligned}&\sigma\Big(\frac{2}{b-a}\Big)^{\alpha}\left(C_1h\sum_{k=1}^{J-j}{}'\frac{V_{j+k}-V_j-z_k\frac{V_{j+1}-V_{j-1}}{2h}}{|z_k|^{1+\alpha}}+C_2h\Big(\sum_{k=-J}^{-1}{}''\frac{V_{j+k}-V_j-z_k\frac{V_{j+1}-V_{j-1}}{2h}}{|z_k|^{1+\alpha}}\right.\\&\left.+\sum_{k=-J-j}^{-J}\frac{V_{j+k}-V_j}{|z_k|^{1+\alpha}}\Big)\right)+\Big(\frac{2}{b-a}\Big(f\Big(\frac{b-a}{2}z_j+\frac{b+a}{2},\varepsilon\Big)+\sigma(C_1-C_2)\frac{\left(\frac{b-a}{2}\right)^{1-\alpha}-1}{1-\alpha}\Big)\end{aligned}$$

$$
\begin{aligned}
&-\sigma\Big(\frac{2}{b-a}\Big)^{\alpha}C_1\frac{1-(1-z_j)^{1-\alpha}}{1-\alpha}\Big)\frac{V_{j+1}-V_{j-1}}{2h}+\Big(\frac{4}{(b-a)^2}\frac{d}{2}-\sigma\Big(\frac{2}{b-a}\Big)^{\alpha}C_{\alpha}\zeta(\alpha-1)\\
&\cdot\frac{1}{2}h^{2-\alpha}\Big)\frac{V_{j+1}-2V_j+V_{j-1}}{h^2}-\sigma\Big(\frac{2}{b-a}\Big)^{\alpha}\frac{V_j}{\alpha}(C_1(1-z_j)^{-\alpha}+C_2(1+z_j)^{-\alpha})\\
=&-\frac{\sigma C_2}{\alpha}\Big(\frac{2}{b-a}\Big)^{\alpha}\Big(z-\frac{2d-b-a}{b-a}\Big)^{-\alpha}\quad\text{for}\quad 0\leqslant j\leqslant J-1,
\end{aligned}\tag{13}
$$

while

$$
\begin{aligned}
&\sigma\Big(\frac{2}{b-a}\Big)^{\alpha}\Big(C_1h\Big(\sum_{k=1}^{J}{}'\frac{V_{j+k}-V_j-z_k\frac{V_{j+1}-V_{j-1}}{2h}}{|z_k|^{1+\alpha}}+\sum_{k=J}^{J-j}\frac{V_{j+k}-V_j}{|z_k|^{1+\alpha}}\Big)+C_2h\sum_{k=-J-j}^{-1}{}''\\
&\cdot\frac{V_{j+k}-V_j-z_k\frac{V_{j+1}-V_{j-1}}{2h}}{|z_k|^{1+\alpha}}\Big)+\Big(\frac{2}{b-a}\Big(f\Big(\frac{b-a}{2}z_j+\frac{b+a}{2},\varepsilon\Big)+\sigma(C_1-C_2)\frac{\big(\frac{b-a}{2}\big)^{1-\alpha}-1}{1-\alpha}\Big)\\
&+\sigma\Big(\frac{2}{b-a}\Big)^{\alpha}C_2\frac{1-(1+z_j)^{1-\alpha}}{1-\alpha}\Big)\frac{V_{j+1}-V_{j-1}}{2h}+\Big(\frac{4}{(b-a)^2}\frac{d}{2}-\sigma\Big(\frac{2}{b-a}\Big)^{\alpha}C_{\alpha}\zeta(\alpha-1)\frac{1}{2}h^{2-\alpha}\Big)\\
&\cdot\frac{V_{j+1}-2V_j+V_{j-1}}{h^2}-\sigma\Big(\frac{2}{b-a}\Big)^{\alpha}\frac{V_j}{\alpha}(C_1(1-z_j)^{-\alpha}+C_2(1+z_j)^{-\alpha})\\
=&-\frac{\sigma C_2}{\alpha}\Big(\frac{2}{b-a}\Big)^{\alpha}\Big(z-\frac{2d-b-a}{b-a}\Big)^{-\alpha}\quad\text{for}\quad -J+1\leqslant j\leqslant -1.
\end{aligned}\tag{14}
$$

For a fixed $\varepsilon\in[\varepsilon_{\text{Fold}\,2},\varepsilon_{\text{Fold}\,1}]$, we take $(a,b)=(x_{U1},x_{S1})$, $(c,d)=[x_{S3},x_{U2}]$, $V_{-J}=V_{x_{U1}}$ and $V_J=0$, and the escape probability $V\triangleq P_2(x)$ corresponding to CT 2 can be obtained via Eqs. (13) and (14). The specific method for choosing $V_{x_{U1}}$ will be introduced below.

4 Absorbed region

Based on Eqs. (9) and (10), $P_1(x)$ of $\forall x\in[x_{U2},x_{S1}]$ or $P_3(x)$ of $\forall x\in[x_{U2},x_{S2}]$ can be obtained. Furthermore, $P_2(x)$ of $\forall x\in[x_{U1},x_{S1}]$ follows from Eqs. (13) and (14). However, it is impossible to determine how large the value of $P_i(x)\,(i=1,2,3)$ is, and the corresponding x is considered to be absorbed into the undesirable state $[x_{S3},x_{U2}]$. To quantify the part of $[x_{U2},x_{S1}]$, $[x_{U1},x_{S1}]$ or $[x_{U2},x_{S2}]$ that may be absorbed into $[x_{S3},x_{U2}]$, the key is to give a threshold value of the corresponding $P_i(x)$. Similar to the method in Ref. [3], the absorbed regions corresponding to CT 1, CT 2, and CT 3 are also defined here via the relationship between the tangent slope of $P_i(x)$ and the slope of a given line in the $xP_i(x)$-plane. It should be noted that, in the following, $\alpha=1.5$, $\beta=-1$, $\sigma=0.8$, and $d=0.1$ are taken as a set of basic parameter values.

4.1 Absorbed region within $[x_{U2},x_{S1}]$ under a fixed $\varepsilon\in[\varepsilon_{\text{Fold}\,4},\varepsilon_{\text{Fold}\,2})$

For CT 1, the given line in the $xP_1(x)$-plane is

$$y_1(x)=\frac{1}{x_{U2}-x_{S1}}x+\frac{x_{S1}}{x_{S1}-x_{U2}},$$

and it is a line connecting $(x_{U2},1)$ and $(x_{S1},0)$. Then, an approximate definition of the absorbed region within $[x_{U2},x_{S1}]$ is given as follows.

Definition 1 *For $\varepsilon\in[\varepsilon_{\text{Fold}\,4},\varepsilon_{\text{Fold}\,2})$, suppose that a tagged partition of $[x_{U2},x_{S1}]$ is a finite sequence $x_{U2}=x_0<x_1<\cdots<x_{L-1}<x_L=x_{S1}$. The set $[x_{U2},x_{L-j}],x_{U2}<x_{L-j}\leqslant x_{S1},j=0,1,\cdots,L-1$ satisfying*

$$\frac{P_1(x_{L-j-1})-P_1(x_{L-j})}{x_{L-j-1}-x_{L-j}}\leqslant\frac{1}{2(x_{U2}-x_{S1})}$$

is defined as the absorbed region D_1 of $[x_{U2},x_{S1}]$ under the Lévy noise.

Based on Definition 1, $P_1(x)$ and D_1 for $\varepsilon = -2.15 \in [\varepsilon_{\text{Fold}\,4}, \varepsilon_{\text{Fold}\,2})$ and different noise parameters are shown in Fig. 2. In addition, the ranges of D_1 corresponding to different α, β, d, and σ are presented in Table 1, respectively. It is found that D_1 within $[x_{U2}, x_{S1}] = [-1.552, 1.711]$ increases with decreasing α. When $\alpha = 1.01$, even the whole $[x_{U1}, x_{S1}]$ becomes D_1 as shown in Fig. 2(a). This is because a smaller α can generate larger jumps which are advantageous for $x \in [x_{U2}, x_{S1}]$ to escape. Furthermore, as shown in Figs. 2(b)–2(d), the range of D_1 also increases with decreasing β or increasing d and σ, which is due to the change of these parameters that can increase the amplitude of the jumps in the Lévy noise.

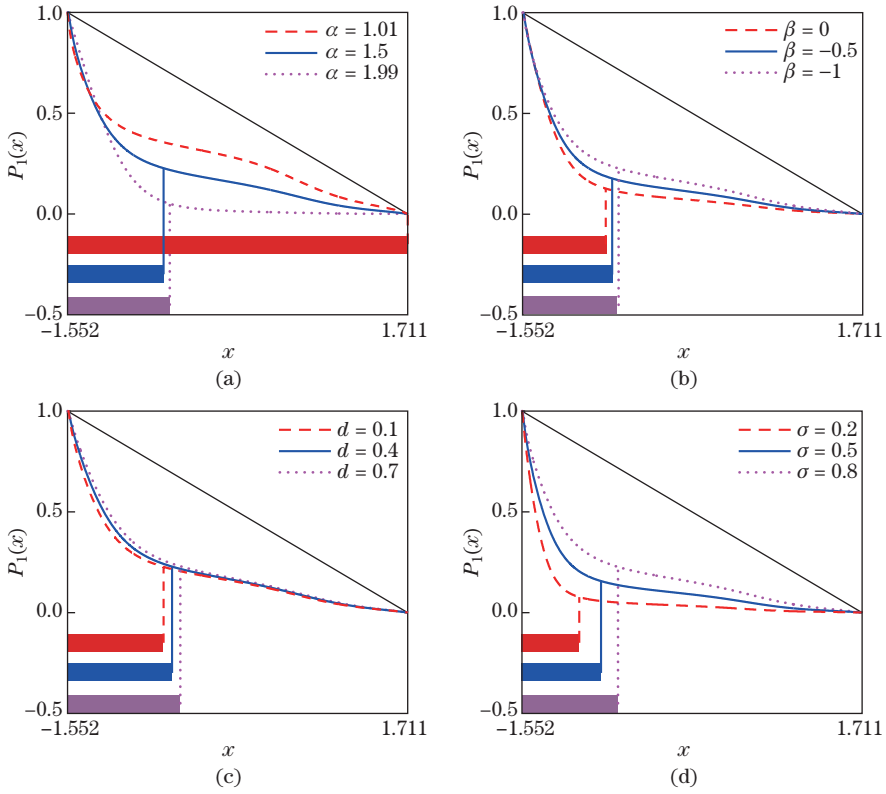

Fig. 2 $P_1(x)$ and the corresponding D_1 (bar-type) for $\varepsilon = -2.15$ and different parameters of the Lévy noise: (a) $\beta = -1$, $\sigma = 0.8$, $d = 0.1$; (b) $\alpha = 1.5$, $\sigma = 0.8$, $d = 0.1$; (c) $\alpha = 1.5$, $\beta = -1$, $\sigma = 0.8$; (d) $\alpha = 1.5$, $\beta = -1$, $d = 0.1$ (color online)

Table 1 The ranges of D_1 under different α, β, d, and σ

ε	α			β		
	1.01	1.5	1.99	−1	−0.5	0
−2.15	$[-1.552, 1.711]$	$[-1.552, -0.629]$	$[-1.552, -0.570]$	$[-1.552, -0.629]$	$[-1.552, -0.691]$	$[-1.552, -0.753]$
ε	d			σ		
	0.1	0.4	0.7	0.2	0.5	0.8
−2.15	$[-1.552, -0.629]$	$[-1.552, -0.549]$	$[-1.552, -0.469]$	$[-1.552, -1.001]$	$[-1.552, -0.792]$	$[-1.552, -0.629]$

4.2 Absorbed region within $[x_{U1}, x_{S1}]$ under a fixed $\varepsilon \in [\varepsilon_{\text{Fold}\,2}, \varepsilon_{\text{Fold}\,1}]$

For CT 2, the given line in the $xP_2(x)$-plane is a line connecting $(x_{U1}, y_2(x_{U1}))$ and $(x_{S1}, 0)$, where

$$y_2(x) = \frac{1}{x_{U2} - x_{S1}} x + \frac{x_{S1}}{x_{S1} - x_{U2}},$$

and $y_2(x_{U1}) = \frac{x_{U1}-x_{S1}}{x_{U2}-x_{S1}}$ is the value when $x = x_{U1}$, as shown in Fig. 3.

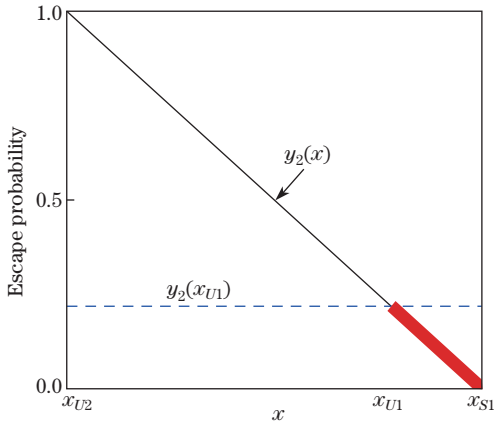

Fig. 3 The given line in the $xP_2(x)$-plane (thick line), where $y_2(x) = \frac{1}{x_{U2}-x_{S1}}x + \frac{x_{S1}}{x_{S1}-x_{U2}}$ is a line connecting $(x_{U2}, 1)$ and $(x_{S1}, 0)$, and the horizontal dotted line is the value of $y_2(x)$ with $x = x_{U1}$ (color online)

Obviously, the given line is a part of $y_2(x)$, and they have the same slope $1/(x_{U2} - x_{S1})$. It should be noted that $y_2(x_{U1})$ is the boundary condition V_{-J} of $P_2(x)$, namely, $V_{-J} = V_{x_{U1}} = y_2(x_{U1})$. Therefore, an approximate definition of the absorbed region within $[x_{U1}, x_{S1}]$ is given as follows.

Definition 2 *For $\varepsilon \in [\varepsilon_{\text{Fold}\,2}, \varepsilon_{\text{Fold}\,1}]$, suppose that a tagged partition of $[x_{U1}, x_{S1}]$ is a finite sequence $x_{U1} = x_0 < x_1 < \cdots < x_{N-1} < x_N = x_{S1}$. The set $[x_{U1}, x_{N-l}], x_{U1} < x_{N-l} \leqslant x_{S1}, l = 0, 1, \cdots, N-1$ satisfying*

$$\frac{P_2(x_{N-l-1}) - P_2(x_{N-l})}{x_{N-l-1} - x_{N-l}} \leqslant \frac{1}{2(x_{U2} - x_{S1})}$$

is defined as the absorbed region D_2 of $[x_{U1}, x_{S1}]$ under the Lévy noise.

Based on Definition 2, $P_2(x)$ and D_2 for $\varepsilon = -1.26 \in [\varepsilon_{\text{Fold}\,2}, \varepsilon_{\text{Fold}\,1}]$ and different noise parameters are shown in Fig. 4. In addition, the ranges of D_2 corresponding to different α, β, d, and σ are presented in Table 2, respectively. In Fig. 4(a), D_2 decreases first and then increases with increasing α, and it is larger especially when α is close to 2. Furthermore, as shown in Figs. 4(b)–4(d), the range of D_2 decreases with decreasing β or increasing d and σ. Obviously, all results here are different from the results in Fig. 2.

In fact, these differences appear because there is a sub-desirable state between the desirable state and the undesirable state. From the energy landscape, a potential well is added between the two potential wells, as shown in Fig. 5. This means that a particle needs to cross two barriers to escape from the desirable state to the undesirable state. When α is smaller and very close to 1, large jumps in the Lévy noise can directly induce a particle to escape to the undesirable state. When α continues to increase, such as $\alpha = 1.5$, the jumps in the Lévy noise cannot directly induce the particle to escape to the undesirable state, while they can induce it to switch between the desirable state and the sub-desirable state. In this case, only the particle stays in the sub-desirable state, namely, it does not go back to the ideal state. Hence, the probability that it escapes to the undesirable state in the next step will increase. Although the decrease of β or increase of d and σ can promote the switching of the particles between the desirable state and the sub-desirable state, it is not sufficient to cause the particles to escape to the undesirable state. On the contrary, the changes of these parameters increase the likelihood that the particles return to the desirable state, and reduce the probability that the particles escape to the undesirable state, as shown in Figs. 4(b)–4(d). When α is further increased to

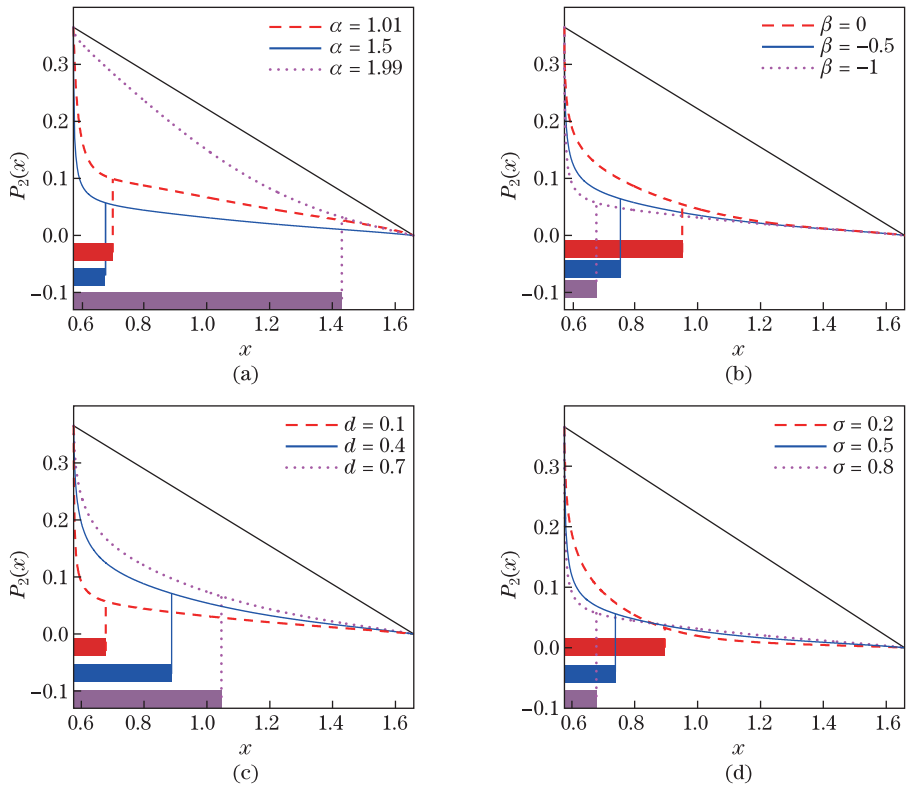

Fig. 4 $P_2(x)$ and the corresponding D_2 (bar-type) for $\varepsilon = -1.26$ and different parameters of the Lévy noise: (a) $\beta = -1$, $\sigma = 0.8$, $d = 0.1$; (b) $\alpha = 1.5$, $\sigma = 0.8$, $d = 0.1$; (c) $\alpha = 1.5$, $\beta = -1$, $\sigma = 0.8$; (d) $\alpha = 1.5$, $\beta = -1$, $d = 0.1$ (color online)

Table 2 The ranges of D_2 under different α, β, d, and σ

ε	α			β		
	1.01	1.5	1.99	−1	−0.5	0
−1.26	[0.576, 0.701]	[0.576, 0.678]	[0.576, 1.430]	[0.576, 0.678]	[0.576, 0.754]	[0.576, 0.951]
ε	d			σ		
	0.1	0.4	0.7	0.2	0.5	0.8
−1.26	[0.576, 0.678]	[0.576, 0.888]	[0.576, 1.046]	[0.576, 0.895]	[0.576, 0.739]	[0.576, 0.678]

be close to 2, the jumps in the Lévy noise gradually decrease. Once a particle escapes to the sub-desirable state, in this case, it becomes difficult to return to the desirable state, which in turn increases the possibility that the particle escapes to the non-ideal state, as shown in Fig. 4(a). As stated above, small perturbations benefit more from the intermediate potential function (the sub-desirable state), while large jumps benefit less[19].

4.3 Absorbed region within $[x_{U2}, x_{S2}]$ under a fixed $\varepsilon \in (\varepsilon_{\text{Fold 1}}, \varepsilon_{\text{Fold 3}}]$

For CT 3, the given line in the $xP_3(x)$-plane is

$$y_3(x) = \frac{1}{x_{U2} - x_{S2}} x + \frac{x_{S2}}{x_{S2} - x_{U2}},$$

and it is a line connecting $(x_{U2}, 1)$ and $(x_{S2}, 0)$. Then, an approximate definition of the absorbed region within $[x_{U2}, x_{S2}]$ is given as follows.

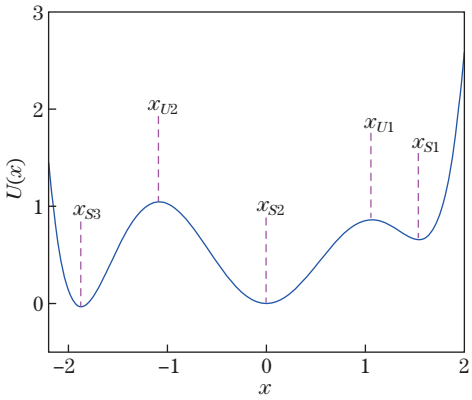

Fig. 5 The general form of the the potential function $U(x)$ of the system (1) with $\varepsilon \in [\varepsilon_{\text{Fold}\,2}, \varepsilon_{\text{Fold}\,1}]$

Definition 3 *For $\varepsilon \in (\varepsilon_{\text{Fold}\,1}, \varepsilon_{\text{Fold}\,3}]$, suppose that a tagged partition of $[x_{U2}, x_{S2}]$ is a finite sequence $x_{U2} = x_0 < x_1 < \cdots < x_{M-1} < x_M = x_{S2}$. The set $[x_{U2}, x_{M-k}], x_{U2} < x_{M-k} \leqslant x_{S2}, k = 0, 1, \cdots, M-1$ satisfying*

$$\frac{P_3(x_{M-k-1}) - P_3(x_{M-k})}{x_{M-k-1} - x_{M-k}} \leqslant \frac{1}{2(x_{U2} - x_{S2})}$$

is defined as the absorbed region D_3 of $[x_{U2}, x_{S2}]$ under the Lévy noise.

Based on Definition 3, $P_3(x)$ and D_3 for $\varepsilon = -0.66 \in (\varepsilon_{\text{Fold}\,1}, \varepsilon_{\text{Fold}\,3}]$ and different noise parameters are shown in Fig. 6. In addition, the ranges of D_3 corresponding to different α,

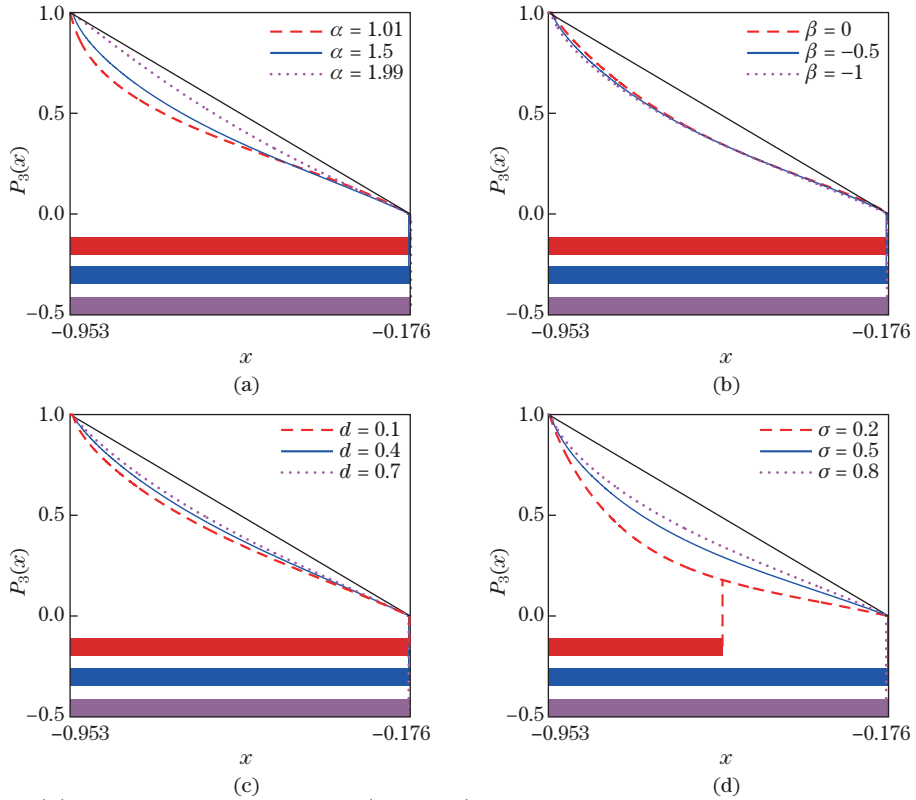

Fig. 6 $P_3(x)$ and the corresponding D_3 (bar-type) for $\varepsilon = 0.66$ and different parameters of the Lévy noise: (a) $\beta = -1$, $\sigma = 0.8$, $d = 0.1$; (b) $\alpha = 1.5$, $\sigma = 0.8$, $d = 0.1$; (c) $\alpha = 1.5$, $\beta = -1$, $\sigma = 0.8$; (d) $\alpha = 1.5$, $\beta = -1$, $d = 0.1$ (color online)

β, d, and σ are presented in Table 3, respectively. The results show that the whole $[x_{U2}, x_{S2}]$ becomes D_3 for different α, β, and d, as shown in Figs. 6(a)–6(c). Furthermore, the whole $[x_{U2}, x_{S2}]$ also becomes D_3 when σ is larger, while a part of it becomes D_3 when $\sigma = 0, 2$, as shown in Fig. 6(d). It indicates that the intensity of Lévy noise plays a key role in the occurrence of CT 3. Although Lévy-noise-induced CT 1 and CT 3 have similar escape problems between two adjacent intervals, CT 3 is more likely to occur because the stability of the current state of the system (1) with $\varepsilon \in (\varepsilon_{\text{Fold}\,1}, \varepsilon_{\text{Fold}\,3}]$ is weaker than the undesirable state.

Table 3 The ranges of D_3 under different α, β, d, and σ

ε	α			β		
	1.01	1.5	1.99	-1	-0.5	0
0.66	$[-0.953, -0.176]$	$[-0.953, -0.176]$	$[-0.953, -0.176]$	$[-0.953, -0.176]$	$[-0.953, -0.176]$	$[-0.953, -0.176]$
ε	d			σ		
	0.1	0.4	0.7	0.2	0.5	0.8
0.66	$[-0.953, -0.176]$	$[-0.953, -0.176]$	$[-0.953, -0.176]$	$[-0.953, -0.555]$	$[-0.953, -0.176]$	$[-0.953, -0.176]$

Although the part of $[x_{U2}, x_{S1}]$, $[x_{U1}, x_{S1}]$ or $[x_{U2}, x_{S2}]$ that may be absorbed into $[x_{S3}, x_{U2}]$ can be quantified, we do not know how large the range of D_i $(i = 1, 2, 3)$ is, and the corresponding asymmetric Lévy-noise-induced CT 1, CT 2 or CT 3 may occur.

5 PDBUR

Supposing that μ is a measurement of the length of an interval, a natural question is how large $\mu(D_1)/\mu([x_{U2}, x_{S1}])$, $\mu(D_2)/\mu([x_{U1}, x_{S1}])$, or $\mu(D_3)/\mu([x_{U2}, x_{S2}])$ is for asymmetric Lévy-noise-induced CT 1, CT 2, or CT 3 to occur. This question will be answered here.

5.1 PDBUR of CT 1

Definition 4 *For D_1 and $[x_{U2}, x_{S1}]$ under $\varepsilon \in (\varepsilon_{Fold\,4}, \varepsilon_{Fold\,2}]$, the set of ε satisfying $\mu_1 \triangleq \frac{\mu(D_1)}{\mu([x_{U2}, x_{S1}])} \geqslant 0.5$ is defined as the PDBUR $U_1(\varepsilon)$ of CT 1 under the Lévy noise.*

Based on Definition 4, Fig. 7 shows the space diagrams of $U_1(\varepsilon)$ of CT 1 corresponding to different parameters of Lévy noise. It is found that, the closer ε is to Fold 2, the larger the range of $U_1(\varepsilon)$ is, which means that CT 1 is more likely to occur. Furthermore, the smaller α, the smaller β, and the larger σ, which are related to the amplitude or the number of the large jumps, can increase the possibility of CT 1 taking place, as shown in Figs. 7(a), 7(b), and 7(d). While d, which describes the intensity of Gaussian, has almost no effect on $U_1(\varepsilon)$, as shown in Fig. 7(c). Anyway, once ε and the noise parameters belong to $U_1(\varepsilon)$, there is a high possibility that CT 1 is impending.

5.2 PDBUR of CT 2

Definition 5 *For D_2 and $[x_{U1}, x_{S1}]$ under $\varepsilon \in (\varepsilon_{\text{Fold}\,2}, \varepsilon_{\text{Fold}\,1}]$, the set of ε satisfying $\mu_2 \triangleq \frac{\mu(D_2)}{\mu([x_{U1}, x_{S1}])} \geqslant 0.5$ is defined as the PDBUR $U_2(\varepsilon)$ of CT 2 under the Lévy noise.*

Based on Definition 5, μ_2 and $U_2(\varepsilon)$ corresponding to asymmetric Lévy-noise-induced CT 2 are shown in Fig. 8. Similarly, CT 2 is more likely to occur when the system (1) is close to Fold 1. Compared with $U_1(\varepsilon)$ in Fig. 7 above or $U_3(\varepsilon)$ in Fig. 9 below, however, the range of $U_2(\varepsilon)$ is very small, especially for β and σ that are related to the amplitude or the number of the large jumps. On the contrary, the range of $U_2(\varepsilon)$ is larger when α is close to 2, namely, there are few jumps in the Lévy noise. Moreover, larger d describing the intensity of the Gaussian also increases the possibility of CT 2 occurring. All results indicate that small perturbations in the Lévy noise are conducive to the occurrence of a CT between non-adjacent states.

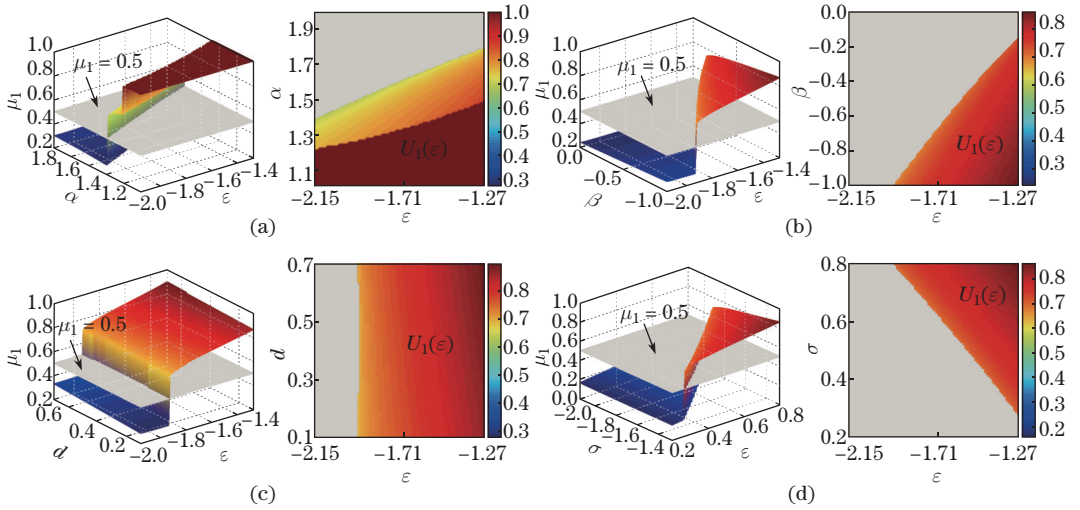

Fig. 7 PDBUR of the asymmetric Lévy-noise-induced CT 1, where the inserted plane represents $\mu_1 = 0.5$: (a) $U_1(\varepsilon)$ under ε versus α; (b) $U_1(\varepsilon)$ under ε versus β; (c) $U_1(\varepsilon)$ under ε versus d; (d) $U_1(\varepsilon)$ under ε versus σ (color online)

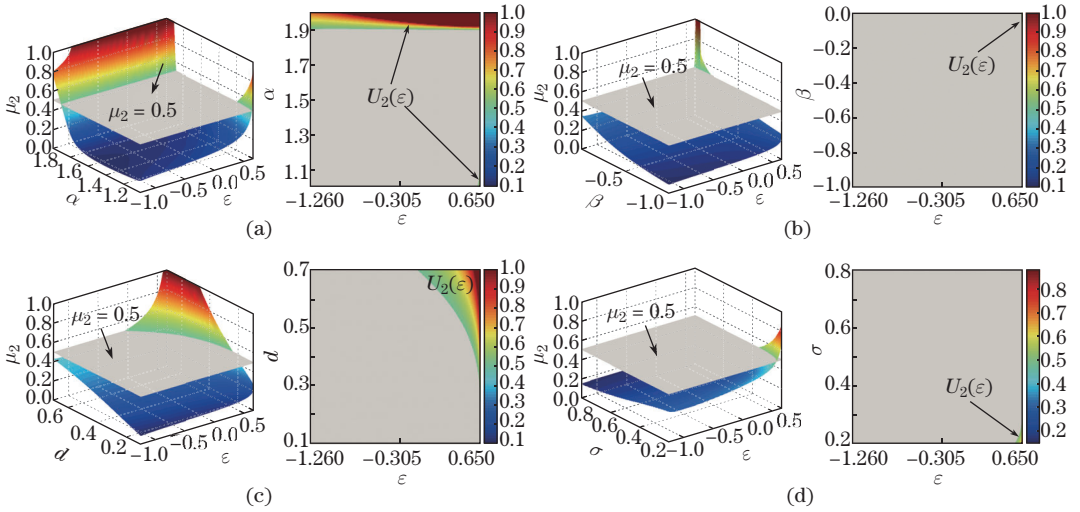

Fig. 8 PDBUR of the asymmetric Lévy-noise-induced CT 2, where the inserted plane represents $\mu_2 = 0.5$: (a) $U_2(\varepsilon)$ under ε versus α; (b) $U_2(\varepsilon)$ under ε versus β; (c) $U_2(\varepsilon)$ under ε versus d; (d) $U_2(\varepsilon)$ under ε versus σ (color online)

Because $V_{x_{U1}} < 1$, $U_2(\varepsilon)$ is different from the PDBUR of CT 1 or CT 3. It does not mean that CT 2 must occur in its region, while it can show that $x \in [x_{U1}, x_{S1}]$ under $\varepsilon \in [\varepsilon_{\text{Fold}\,2}, \varepsilon_{\text{Fold}\,1}]$ has a high probability of escaping to the undesirable state relative to the boundary condition $V_{x_{U1}}$. However, the quantization of the PDBUR of CT 2 can guide us in preventing a catastrophic CT.

5.3 PDBUR of CT 3

Definition 6 *For D_3 and $[x_{U2}, x_{S2}]$ under $\varepsilon \in [\varepsilon_{Fold\,1}, \varepsilon_{Fold\,3}]$, the set of ε satisfying $\mu_3 \triangleq \frac{\mu(D_3)}{\mu([x_{U2}, x_{S2}])} \geqslant 0.5$ is defined as the PDBUR $U_3(\varepsilon)$ of CT 3 under the Lévy noise.*

Based on Definition 6, the space diagrams of $U_3(\varepsilon)$ of asymmetric Lévy-noise-induced CT 3 are shown in Fig. 9. Obviously, all the regions of ε versus α, ε versus β, ε versus d, and ε versus

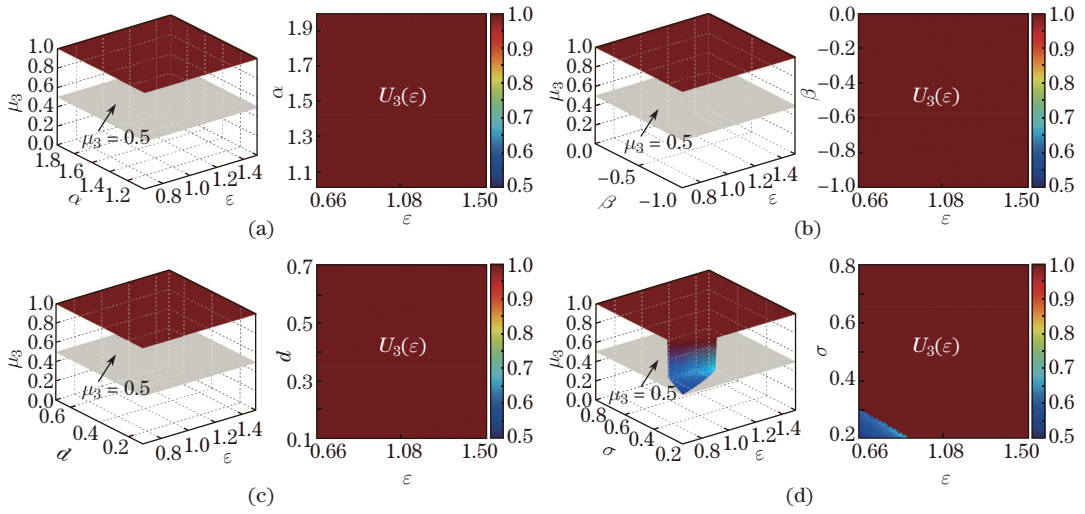

Fig. 9 PDBUR of the asymmetric Lévy-noise-induced CT 3, where the inserted plane represents $\mu_3 = 0.5$: (a) $U_3(\varepsilon)$ under ε versus α; (b) $U_3(\varepsilon)$ under ε versus β; (c) $U_3(\varepsilon)$ under ε versus d; (d) $U_3(\varepsilon)$ under ε versus σ (color online)

σ become $U_3(\varepsilon)$ under the given set of basic parameter values. This means that the Lévy noise can easily induce CT 3 to occur in $\varepsilon \in (\varepsilon_{\text{Fold}\,1}, \varepsilon_{\text{Fold}\,3}]$. Moreover, our results show that μ_3 is less than 1 when σ is small, that is, $[x_{U2}, x_{S2}]$ does not all become the absorbed region. Therefore, σ plays an important role in this case. Our goal is to avoid ε and the noise parameters entering $U_3(\varepsilon)$ in practical systems.

6 Conclusions

In this paper, we have focused on an asymmetric Lévy-noise-induced tri-stable model as a concrete example to quantify the ranges of the parameters where CTs from the desirable state directly to the undesirable state may occur. Based on the escape probability, the absorbed regions that the current state of the given model is absorbed into the undesirable state corresponding to CT 1, CT 2, and CT 3 are first defined. Then, the concept of the PDBUR under the asymmetric Lévy noise is introduced. Once the control parameter and the noise parameters enter the PDBUR of CT 1, CT 2, or CT 3, there is a high possibility that a catastrophic CT is impending. Now, some managements should be adopted to avert it.

However, in the definitions of the absorbed region and the PDBUR, the scale factor is taken as 1/2. More accurate results may be realized in terms of other values, which need to be further explored and developed. Moreover, we take $\alpha = 1.5$, $\beta = -1$, $\sigma = 0.8$, and $d = 0.1$ as a set of basic parameter values in the calculation. Figures 6 and 9 have shown that the current state of the given model is not all absorbed into the undesirable state when σ is smaller, such as $\sigma = 0.2$. Therefore, more interesting phenomena may be obtained for other basic parameter values. Our method may be regarded as a complement to existing early warning indicators, and more general methods need to be established.

References

[1] SCHEFFER, M., CARPENTER, S., FOLEY, J. A., FOLKE, C., and WALKER, B. Catastrophic shifts in ecosystems. *nature*, **413**, 591–596 (2001)

[2] MA, J. Z., XU, Y., XU, W., LI, Y. G., and KURTHS, J. Slowing down critical transitions via Gaussian white noise and periodic force. *Science China Technological Sciences*, **62**, 2144–2152 (2019)

[3] MA, J. Z., XU, Y., LI, Y. G., TIAN, R. L., and KURTHS, J. Predicting noise-induced critical transitions in bistable systems. *Chaos*, **29**, 081102 (2019)

[4] ZHANG, X. Y., XU, Y., LIU, Q., and KURTHS, J. Rate-dependent tipping-delay phenomenon in a thermoacoustic system with colored noise. *Science China Technological Sciences*, **63**, 2315–2327 (2020)

[5] SCHEFFER, M., BASCOMPTE, J., BROCK, W. A., BROVKIN, V., CARPENTER, S. R., DAKOS, V., HELD, H., VAN NES, E. H., RIETKERK, M., and SUGIHARA, G. Early-warning signals for critical transitions. *nature*, **461**, 53–59 (2009)

[6] DASILIS, V., CARPENTER, S. R., BROCK, W. A., ELLISON, A. M., GUTTAL, V., IVES, A. R., KÉFI, S., LIVINA, V., SEEKELL, D. A., VAN NES, E. H., and SCHEFFER, M. Methods for detecting early warnings of critical transitions in time series illustrated using simulated ecological data. *PLoS One*, **7**, e41010 (2012)

[7] WILLIAMSON, M. S., BATHIANY, S., and LTNTON, T. M. Early warning signals of tipping points in periodically forced systems. *Earth System Dynamics*, **7**, 313–326 (2016)

[8] MA, J. Z., XU, Y., KURTHS, J., WANG, H. Y., and XU, W. Detecting early-warning signals in periodically forced systems with noise. *Chaos*, **28**, 113601 (2018)

[9] AO, P., GALAS, D., HOOD, L., and ZHU, X. M. Cancer as robust intrinsic state of endogenous molecular-cellular network shaped by evolution. *Medical Hypotheses*, **70**, 678–684 (2008)

[10] BARNOSKY, A. D., HADLY, E. A., BASCOMPTE, J., BERLOW, E. L., BROWN, J. H., FORTELIUS, M., GETZ, W. M., HARTE, J., HASTINGS, A., MARQUET, P. A., MARTINEZ, N. D., MOOERS, A., ROOPNARINE, P., VERMEIJ, G., WILLIAMS, J. W., GILLESPIE, R., KITZES, J., MARSHALL, C., MATZKE, N., MINDELL, D. P., REVILLA, E., and SMITH, A. B. Approaching a state shift in Earth's biosphere. *nature*, **486**, 52–58 (2012)

[11] STOLBOVA, V., SUROVYATKINA, E., BOOKHAGEN, B., and KURTHS, J. Tipping elements of the Indian monsoon: prediction of onset and withdrawal. *Geophysical Research Letters*, **43**, 3982–3990 (2016)

[12] SU, C. H. and ZHOU, H. Stability analysis and transition prediction of hypersonic boundary layer over a blunt cone with small nose bluntness at zero angle of attack. *Applied Mathematics and Mechanics* (*English Edition*), **28**, 563–572 (2007) https://doi.org/10.1007/s10483-007-0501-1

[13] HAN, Y. F. and CAO, W. Flat-plate hypersonic boundary-layer flow instability and transition prediction considering air dissociation. *Applied Mathematics and Mechanics* (*English Edition*), **40**, 719–736 (2019) https://doi.org/10.1007/s10483-019-2480-6

[14] YUAN, R. S., ZHU, X. M., WANG, G. W., LI, S. T., and AO, P. Cancer as robust intrinsic state shaped by evolution: a key issues review. *Reports on Progress in Physics*, **80**, 042701 (2017)

[15] ZHENG, Y. and HUANG, J. H. Stochastic stability of FitzHugh-Nagumo systems perturbed by Gaussian white noise. *Applied Mathematics and Mechanics* (*English Edition*), **32**, 11–22 (2011) https://doi.org/10.1007/s10483-011-1389-7

[16] MEI, R. X., XU, Y., LI, Y. G., and KURTHS, J. The steady current analysis in a periodic channel driven by correlated noises. *Chaos, Solitons and Fractals*, **135**, 109766 (2020)

[17] LI, Y. G., MEI, R. X., XU, Y., KURTHS, J., DUAN, J. Q., and METZLER, R. Particle dynamics and transport enhancement in a confined channel with position-dependent diffusivity. *New Journal of Physics*, **22**, 053016 (2020)

[18] FOGEBDY, H. C. Lévy flights in random environments. *Physical Review Letters*, **73**, 2517–2520 (1994)

[19] WANG, Z. Q., XU, Y., and YANG, H. Lévy noise induced stochastic resonance in an FHN model. *Science China Technological Sciences*, **59**, 371375 (2016)

[20] PADASH, A., CHECHKIN, A. V., DYBIEC, B., PAVLYUKEVICH, I., SHOKRI, B., and METZLER, R. First-passage properties of asymmetric Lévy flights. *Journal of Physics A—Mathematical and Theoretical*, **52**, 454004 (2019)

[21] XU, Y., ZAN, W. R., JIA, W. T., and KURTHS, J. Path integral solutions of the governing equation of SDEs excited by Lévy white noise. *Journal of Computational Physics*, **394**, 41–55 (2019)

[22] MANTEGNA, R. and STANLEY, E. Scaling behaviour in the dynamics of an economic index. *nature*, **376**, 46–49 (1995)

[23] SCHOUTENS, W. Exotic options under Lévy models: an overview. *Journal of Computational and Applied Mathematics*, **189**, 526–538 (2006)

[24] LI, Y. G., XU, Y., KURTHS, J., and YUE, X. L. Lévy-noise-induced transport in a rough triple-well potential. *Physical Review E*, **94**, 042222 (2016)

[25] LOMHOLT, M. A., AMBJÖRNSSON, T., and METZLER, R. Optimal target search on a fast-folding polymer chain with volume exchange. *Physical Review Letters*, **95**, 260603 (2005)

[26] PALYULIN, V. V., BLACKBURN, G., LOMHOLT, M. A., WATKINS, N. W., METZLER, R., KLAGES, R., and CHECHKIN, A. V. First passage and first hitting times of Lévy flights and Lévy walks. *New Journal of Physics*, **21**, 103028 (2019)

[27] WOYCZYŃSKI, W. A. *Lévy Processes in the Physical Sciences*, Birkhäuser, Boston, MA (2001)

[28] DITLEVSEN, P. D. Observation of α-stable noise induced millennial climate changes from an ice-core record. *Geophysical Research Letters*, **26**, 1441–1444 (1999)

[29] MA, J. Z., XU, Y., LI, Y. G., TIAN, R. L., CHEN, G. R., and KURTHS, J. Precursor criteria for noise-induced critical transitions in multi-stable systems. *Nonlinear Dynamics*, **101**, 21–35 (2020)

[30] WANG, X., DUAN, J. Q., LI, X. F., and SONG, R. M. Numerical algorithms for mean exit time and escape probability of stochastic systems with asymmetric Lévy motion. *Applied Mathematics and Computation*, **337**, 618–634 (2018)

[31] SIDI, A. and ISRAELI, M. Quadrature methods for periodic singular and weakly singular Fredholm integral equations. *Journal of Scientific Computing*, **3**, 201–231 (1988)

[32] GAO, T., DUAN, J. Q., LI, X. F., and SONG, R. M. Mean exit time and escape probability for dynamical systems driven by Lévy noises. *SIAM Journal on Entific Computing*, **36**, A887–A906 (2014)

[33] ZHENG, Y. Y., SERDUKOVA, L., DUAN, J. Q., and KURTHS, J. Transitions in a genetic transcriptional regulatory system under Lévy motion. *Scientific Reports*, **6**, 29274 (2016)